Ligand Interactions in the Distal Heme Pocket of *Mycobacterium tuberculosis* Truncated Hemoglobin N: Roles of TyrB10 and GlnE11 Residues†

Yannick Ouellet,‡ Mario Milani,§ Manon Couture,‡ Martino Bolognesi,§,|| and Michel Guertin*,‡

Department of Biochemistry and Microbiology, Laval University, Quebec, Canada, G1K 7P4, CNR-INFM, Milano Research Unit, Milano I-20131, Italy, and Department of Biomolecular Sciences and Biotechnology, University of Milano, Milano I-20131, Italy

Received January 18, 2006; Revised Manuscript Received May 17, 2006

ABSTRACT: The crystallographic structure of oxygenated trHbN from *Mycobacterium tuberculosis* showed an extended heme distal site hydrogen-bonding network that includes Y(B10), Q(E11), and the bound O_2 (Milani, M., et al. (2001) *EMBO J. 20*, 3902−3909). In the present work, we analyze the effects that substitutions at the B10 and E11 positions exert on the heme and its coordinated ligands, using steady-state resonance Raman spectroscopy, absorption spectroscopy and X-ray crystallography. Our results show that (1) residues Y(B10) and Q(E11) control the binding and the ionization state of the heme-bound water molecules in ferric trHbN and are important in keeping the sixth coordination position vacant in deoxy trHbN; (2) residue Q(E11) plays a role in maintaining the integrity of the proximal Fe−His bond in deoxy trHbN; (3) in wild-type oxy-trHbN, the size and hydrogen-bonding capability of residue E11 is important to sustain proper interaction between Y(B10) and the heme-bound O_2; (4) CO-trHbN is in a conformational equilibrium, where either the Y(B10) or the Q(E11) residue interacts with the heme-bound CO; and (5) Y(B10) and Q(E11) residues control the conformation (and likely the dynamics) of the protein matrix tunnel gating residue F(E15). These findings suggest that the functional processes of ligand binding and diffusion are controlled in trHbN through the dynamic interaction of residues Y(B10), Q(E11), F(E15), and the heme ligand.

TrHbN belongs to the truncated hemoglobin (trHb[1]) family, a member of the hemoglobin (Hb) superfamily (*1*−*3*). TrHbN is one of the two trHbs expressed in *Mycobacterium tuberculosis*, and trHbN is expressed in vitro during the stationary phase of *M. tuberculosis* (*4*). It binds oxygen with high affinity (P_{50} = 0.013 mmHg) because of a fast combination (25 μM^{-1} s^{-1}) and a very low ligand dissociation rate (k_{off} = 0.2 s^{-1}) (*4*). Inactivation of the *glbN* gene impairs the ability of stationary phase cells to protect aerobic respiration from NO inhibition, suggesting that trHbN may play a vital role in protecting *M. tuberculosis* from NO toxicity in vivo (*5*). This functional assessment is supported by the observation that trHbN catalyzes the rapid oxidation of nitric oxide (NO) to nitrate (trHbN−$Fe^{2+}O_2$ + NO → trHbN−Fe^{3+} + NO_3^-), with a second-order rate constant $k \approx 745$ μM^{-1} s^{-1} (23 °C) (*5*).

In contrast with the situation observed in vertebrate myoglobins and Hbs, the tertiary structure of trHbN as well as those of other trHbs studied by X-ray crystallography show the presence of extended heme distal site hydrogen-bonding networks that, according to the context, may include the heme-bound ligand (*1*, *6*−*10*). Parallel spectroscopic studies also provide indication of distal site hydrogen-bonding networks in other trHbs (*11*−*15*). The heme-bound O_2 molecule of oxygenated trHbN is hydrogen-bonded to the Y(B10) phenolic O atom, which also forms a hydrogen bond with the N atom of Q(E11) (Figure 6A). The same network based on Y(B10)/Q(E11) hydrogen bonds is observed in the crystal structure of the ferric-cyano form of trHbN (Figure 6B and ref 16) (*16*), supporting the idea that such distal site hydrogen-bonding network is instrumental for ligand binding and stabilization. Accordingly, a kinetic analysis of the Y(B10)F mutant, where hydrogen-bonding capabilities are partly impaired, showed a 150-fold increase in the O_2 dissociation rate (*4*). Furthermore, protection against NO toxicity could not be restored when cells containing the inactivated *glbN* gene were transformed with a plasmid expressing the Y(B10)F trHbN mutant, pointing to a crucial role for the heme distal site residue Y(B10) in NO detoxification (*5*).

† This work was supported by the National Sciences and Engineering Research Council (NSERC) grant 46306-01 (2005−2010) and NIH grant 1-R01-AI052258 (2004-2007) to Dr. Michel Guertin. Mario Milani is the recipient of a postdoctoral fellowship supported by NIH grant 1-R01-AI052258 (2004−2007). Dr. Manon Couture is supported by NSERC grant 250073 and the Fonds Québécois de la Recherche sur la Nature et les Technologies (FQRNT) grant 78927. Dr. Martino Bolognesi is grateful to CIMAINA (Milano, Italy) and to Fondazione Compagnia di San Paolo (Torino, Italy) for continuous support. Part of this study was supported by the Italian Ministry for University and Scientific Research FIRB Project "Biologia Strutturale" to Dr. Martino Bolognesi, Contract RBLA03B3KC.

* Corresponding author: Tel: 418-656-2131 ext. 5581. Fax: 418-656-7176. E-mail: Michel.Guertin@rsvs.ulaval.ca.

‡ Laval University.

§ CNR-INFM.

|| University of Milano.

[1] Abbreviations: BCG, bacillus Calmette−Guérin; Hb, hemoglobin; trHb, truncated hemoglobin; trHbN, truncated hemoglobin N; 4C, four-coordinated; 5C, five-coordinated; 6C, six-coordinated; sh, shoulder; HMP, hemoglobin-like protein.

10.1021/bi060112o CCC: $33.50
Published on Web 06/28/2006

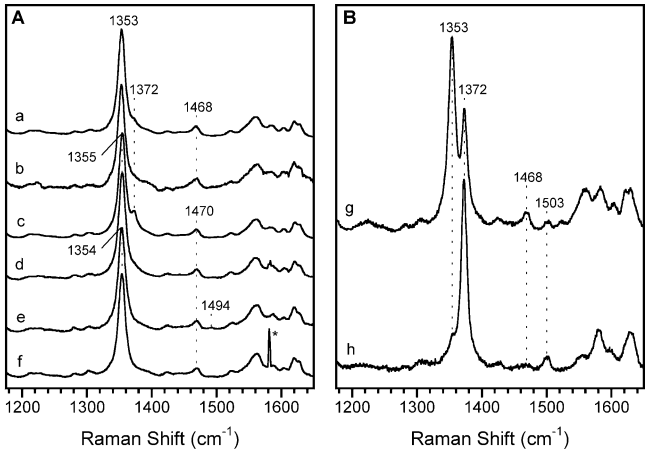

FIGURE 1: Resonance Raman spectra of the deoxy forms of trHbN and its mutants at pH 7.5 (A) and pH 5 (B) in the high-frequency region. (A) a, trHbN; b, Y(B10)F; c, Q(E11)A; d, Q(E11)V; e, Y(B10)F/Q(E11)V; and f, Y(B10)L/Q(E11)V recorded at pH 7.5. (B) g, trHbN and h, Q(E11)A recorded at pH 5. All spectra were obtained with 441.6 nm excitation. The asterisk marks the laser band.

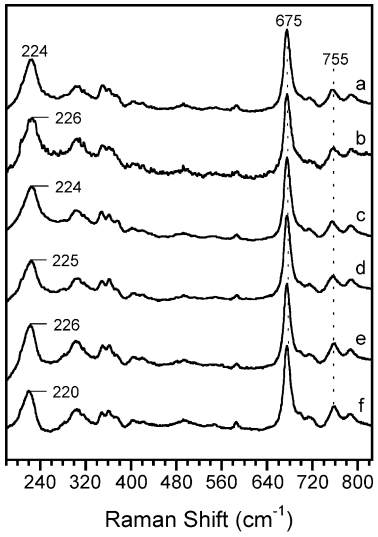

FIGURE 2: Resonance Raman spectra of the deoxy forms of trHbN and its mutants at pH 7.5 in the low-frequency region. a, trHbN; b, Y(B10)F; c, Q(E11)A; d, Q(E11)V; e, Y(B10)F/Q(E11)V; and f, Y(B10)L/Q(E11)V recorded at pH 7.5.

The role of residue Q(E11) within the heme distal site hydrogen-bonding network has not been investigated yet. Nevertheless, a recent analysis of geminate rebinding of CO in the sol−gel encapsulated wild-type trHbN and the Y(B10)F mutant strongly suggested that interactions between Y(B10) and Q(E11) influence the relaxation properties of the distal heme pocket, thus affecting ligand rebinding kinetics (*17*). In addition, classical and hybrid quantum-classical simulations indicated that the Y(B10)−Q(E11) pair would modulate the affinity for O_2 and NO, playing a dominant role in the NO oxidation reaction (*18*).

In the present study, we replaced *M. tuberculosis* trHbN Y(B10) and Q(E11) with nonpolar residues and characterized the mutant proteins by absorption spectroscopy, resonance Raman spectroscopy, and X-ray crystallography. Our results show that both Y(B10) and Q(E11) residues interact with the heme-bound ligands, while fine modulating the resulting protein/ligand interaction processes. Our results also suggest that these two distal residues may exert a control on the conformation, and possibly the dynamics of residue F(E15), which we previously proposed acts as a gating residue within

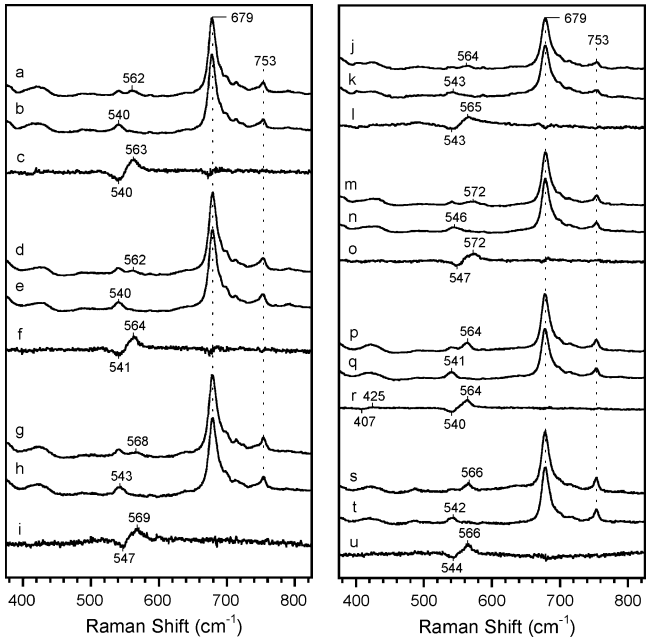

FIGURE 3: Low-frequency region of the resonance Raman spectra of the O_2 derivatives of trHbN and its mutants. a, trHbN-$^{16}O_2$; b, trHbN-$^{18}O_2$; d, Q(E11)A-$^{16}O_2$; e, Q(E11)A-$^{18}O_2$; g, Q(E11)V-$^{16}O_2$; h, Q(E11)V-$^{18}O_2$; j, Y(B10)F-$^{16}O_2$; k, Y(B10)F-$^{18}O_2$; m; Y(B10)L-$^{16}O_2$; n, Y(B10)L-$^{18}O_2$; p, Y(B10)F/Q(E11)V-$^{16}O_2$; q, Y(B10)F/Q(E11)V-$^{18}O_2$; s, Y(B10)L/Q(E11)V-$^{16}O_2$; t, Y(B10)L/Q(E11)V-$^{18}O_2$; c, f, i, l, o, r, and u correspond to the difference spectra ^{16}O minus ^{18}O for each protein.

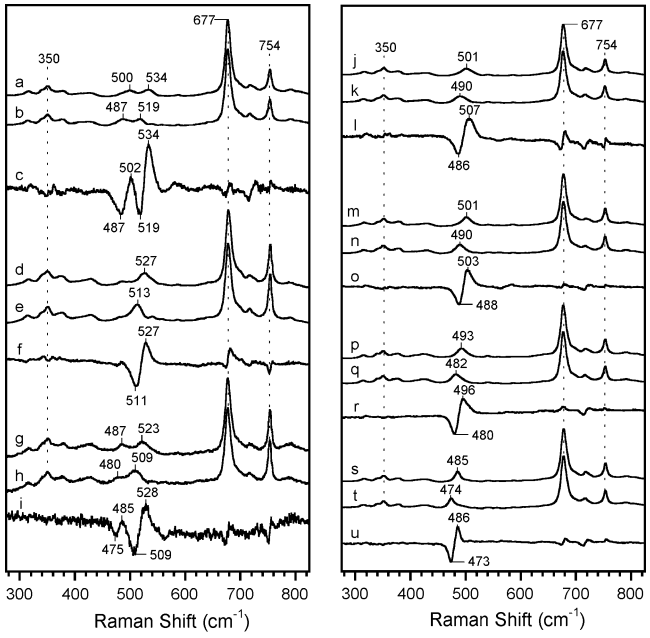

FIGURE 4: Resonance Raman spectra of the CO derivatives in the low-frequency region of trHbN and its mutants. a, trHbN-$^{12}C^{16}O$; b, trHbN-$^{13}C^{18}O$; d, Q(E11)A-$^{12}C^{16}O$; e, Q(E11)A-$^{13}C^{18}O$; g, Q(E11)V-$^{12}C^{16}O$; h, Q(E11)V-$^{13}C^{18}O$; j, Y(B10)F-$^{12}C^{16}O$; k, Y(B10)F-$^{13}C^{18}O$; m; Y(B10)L-$^{12}C^{16}O$; n, Y(B10)L-$^{13}C^{18}O$; p, Y(B10)F/Q(E11)V-$^{12}C^{16}O$; q, Y(B10)F/Q(E11)V-$^{13}C^{18}O$; s, Y(B10)L/Q(E11)V-$^{12}C^{16}O$; t, Y(B10)L/Q(E11)V-$^{13}C^{18}O$; c, f, i, l, o, r, and u correspond to the difference spectra $^{12}C^{16}O$ minus $^{13}C^{18}O$ for each protein.

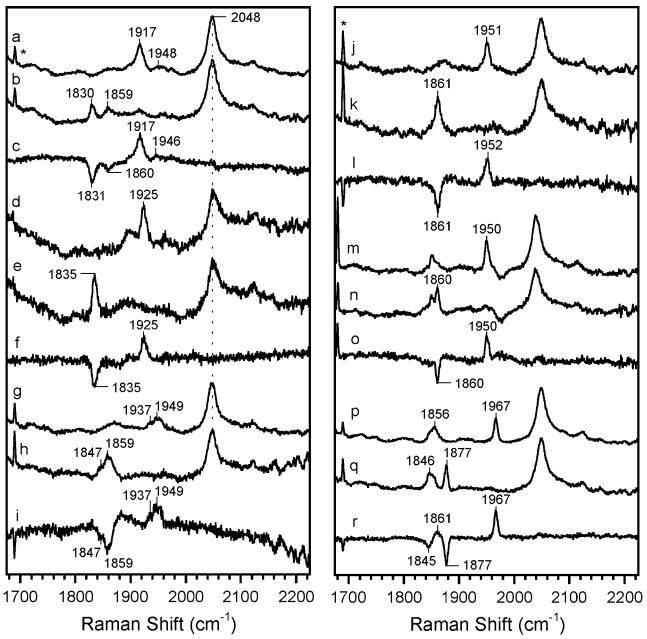

FIGURE 5: Resonance Raman spectra of the CO derivatives in the high-frequency region of trHbN and its mutants. a, trHbN-$^{12}C^{16}O$; b, trHbN-$^{13}C^{18}O$; d, Q(E11)A-$^{12}C^{16}O$; e, Q(E11)A-$^{13}C^{18}O$; g, Y(B10)F-$^{12}C^{16}O$; h, Y(B10)F-$^{13}C^{18}O$; j, Y(B10)L-$^{12}C^{16}O$; k, Y(B10)L-$^{13}C^{18}O$; m, Y(B10)F/Q(E11)V-$^{12}C^{16}O$; n, Y(B10)F/Q(E11)V-$^{13}C^{18}O$; p, Y(B10)L/Q(E11)V-$^{12}C^{16}O$; q, Y(B10)L/Q(E11)V-$^{13}C^{18}O$; c, f, i, l, o and r correspond to the difference spectra $^{12}C^{16}O$ minus $^{13}C^{18}O$ for each protein. The asterisk marks the laser band.

a trHbN protein matrix tunnel suited for ligand diffusion to/from the heme (*7*).

MATERIAL AND METHODS

Mutagenesis, Expression and Purification. Amino acid substitutions were performed on the *glbN* gene using the Stratagene QuickChange Site-Directed Mutagenesis protocol. The expression and purification of the recombinant proteins were performed in accordance with the previously published method (*14*) except that $FeCl_3$ (250 μM) and hemin chloride (10 μg/mL) were added to the growth medium.

Optical Absorption Spectroscopy. Optical absorption spectra were recorded using a Cary 3E spectrophotometer (Varian) equipped with a temperature-controlled multicell holder. Ferric samples were prepared at room temperature by the addition of a few grains of potassium ferricyanide to the oxy form. After allowing the reaction to proceed to completion, the proteins were purified by desalting over a P6DG column equilibrated with 10 mM Tris-Cl at pH 7.5 and 50 μM EDTA and were dialyzed overnight against 10 mM Tris-Cl at pH 7.5 and 50 μM EDTA at 4 °C. The deoxy samples were prepared from the ferric form inside an anaerobic chamber (Labmaster 100, MBraun) by injecting a 10-fold molar excess of sodium dithionite. The deoxy proteins were desalted over a P-6DG column equilibrated with 50 mM potassium phosphate at pH 7.5 and 50 μM EDTA. Oxy and CO samples were prepared by exposing the deoxy proteins to either air or CO. All spectra were recorded at 10 μM and 23 °C and analyzed using the Kaleidagraph software (Synergy Software).

Resonance Raman Spectroscopy. Protein samples for the Raman experiments were used at a concentration of 50 μM and were buffered in 50 mM potassium phosphate at pH 7.5 containing 50 μM EDTA. Acidic protein samples were prepared in 50 mM sodium acetate at pH 5 containing 50 μM EDTA. The deoxy protein samples were prepared by injecting a 10-fold molar excess of sodium dithionite, freshly prepared from anaerobic solutions, to argon-equilibrated protein samples in tightly sealed Raman cells. CO derivatives were prepared by exposing argon-equilibrated, dithionite-reduced protein samples to either $^{12}C^{16}O$ (MEGS inc, Quebec, CA) or $^{13}C^{18}O$ (Icon Isotopes, Summit, NJ). To obtain the O_2 derivatives, the deoxy protein samples were prepared inside the anaerobic chamber as described above. The O_2 derivatives were prepared by injecting either $^{16}O_2$ (Praxair, Quebec, CA) or $^{18}O_2$ (Cambridge Isotopes Laboratories, Andover, MA) to the dithionite-free deoxy protein samples. Absorption spectra were recorded before and after each experiment to ensure the integrity of the samples. The resolution of the Raman instrumentation was 1 cm^{-1} (*19*). The output at 441.6 nm from a He/Cd laser and 413.1 nm from a krypton ion laser were used to acquire the spectra of the deoxy derivatives. The excitation source for the acquisition of the O_2 and CO spectra was the 406.7 and 413.1 nm lines of a krypton ion laser maintained at a power of less than 2 mW to minimize ligand dissociation. The resonance Raman spectra were calibrated with the lines of indene in the 200−1700 cm^{-1} range and from acetone and ferrocyanide in the 1700−2300 cm^{-1} range. All measurements were made at room temperature. Cosmic ray lines were removed from the spectra by a routine of Winspec software (Roper Scientific, Princeton, NJ). Several 5 min spectra were acquired over a 30 min period and analyzed using the Grams/AI software (ThermoGalactic).

X-ray Crystallography. All trHbN mutants were crystallized using the hanging drop setup, as their cyano-met forms, applying crystallization conditions close to those reported for the wild-type oxy-trHbN (*7*). For crystallization, the protein solution was modified by the addition of 10 mM potassium ferricyanide and 1 mM KCN; crystal growth was achieved by mixing 1−2 μL of the appropriate protein solution (30−35 mg/mL) with 1 μL of the reservoir containing K_2HPO_4/NaH_2PO_4 1.7−1.8 M at pH 7.6−8.1. The crystals, grown in about two weeks, were transferred and conserved in the stabilizing medium (K_2HPO_4/NaH_2PO_4 2 M, KCN 1 mM) at 4° C and plunged in the same solution supplemented with 20% glycerol before X-ray data collections at ESRF beam lines ID14-1, ID14-3, and at DESY Hamburg beam line BW7B. Diffraction data reduction and crystallographic computing were based on DENZO or Mosflm and on programs from the CCP4 suite, respectively (*20*, *21*). After rigid body refinement of the oxy-trHbN model (pdb entry 1IDR) against the individual datasets (*22*), the four mutant trHbN structures were refined/inspected using Refmac5 and O (*23*, 24). Data collection and refinement statistics are reported in Table 2. Atomic coordinates and structure factors for the trHbN mutants[2] reported here have been deposited with the Protein Data Bank (*25*) from which they can be recovered.

[2] The PDB entry codes for the cyano-met structures are 2gln (Q(E11)A), 2gkn (Q(E11)V), 2gkm (Y(B10)F), and 2gl3 (Y(B10)F/Q(E11)V).

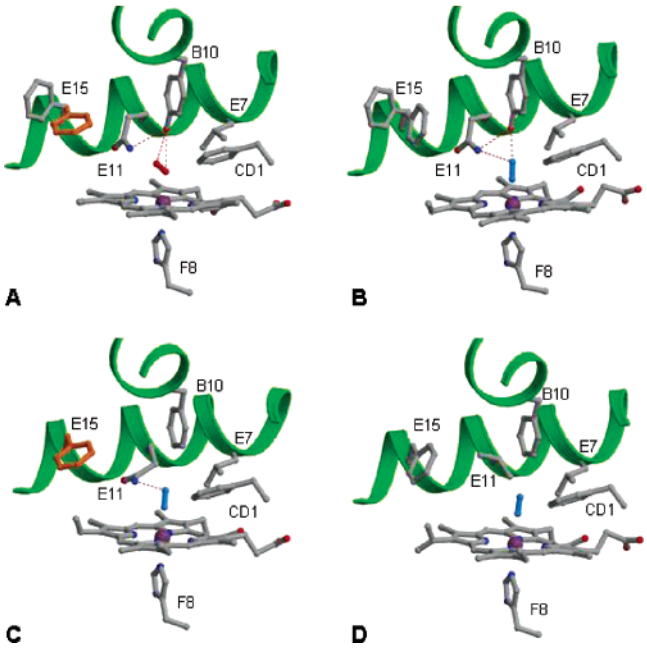

FIGURE 6: Three-dimensional structure of trHbN in the heme distal site region of the wild-type protein and selected mutants. (A) Mono view of the distal site region for wild-type trHbN, showing the O_2-liganded heme group (the heme-Fe atom is purple), portions of the B and E helices, the distal residues at sites B10, CD1, and E7−E11 in the surrounding structural region. Residue F(E15), gating the intramolecular tunnel of trHbN, is shown in the two conformations (open, orange; closed, gray) observed in the wild-type protein. (B) Heme distal site region of the cyano-met wild-type trHbN displayed in the same orientation and following the same conventions as those in panel A. (C) Heme distal site region of the cyano-met trHbN Y(B10)F mutant. (D) Heme distal region of cyano-met trHbN Y(B10)F/Q(E11)V trHbN double mutant, portrayed in the same orientation and following the same conventions as those in panel A. The hydrogen bonds are shown as dashed lines. The heme ligands are shown in red (for O_2) and cyan (for cyanide) (drawn with Molscript (*55*, *56*)).

RESULTS

Optical Absorption Spectra of the Ferric and Deoxy Derivatives. The optical absorption spectrum of ferric wild-type trHbN is typical of a high-spin hexacoordinate (6C) heme species, at pH 7.5, with a minor contribution from a 6C low-spin species, as revealed by the positioning of the Soret band at 405.5 nm and the maxima at 502, 542 (sh), 585 (sh), and 632 nm in the visible region (*4*). Changing the Y(B10) residue for a phenylalanine or a leucine resulted in spectra almost identical to that of wild-type trHbN (*4*). On the contrary, the absorption spectra of the ferric Q(E11) mutants revealed a single 6C low-spin species as shown by the wavelength maxima at 413, 546, and 578 nm for the Q(E11)A mutant and 410, 545, 580, and 628 nm (sh) for the Q(E11)V mutant (Figure 1 Supporting Information). Interestingly, the optical spectra of the ferric complex of the double mutants were mostly 5C as indicated by the electronic transitions at 380 (sh), 397.5, 505, 539 (sh), and 641 nm for the Y(B10)F/Q(E11)V mutant and 393, 505, 538 (sh), and 643 nm for the Y(B10)L/Q(E11)V mutant (Figure 1 Supporting Information).

The optical absorption spectra at pH 7.5 of deoxy wild-type trHbN (Figure 2 Supporting Information) as well as those of the deoxy Y(B10) and the Q(E11) single mutants (not shown) revealed the presence of five-coordinate (5C) complexes with maxima at 432 and 556 nm. The deoxy spectra of the double mutants showed blue-shifted Soret bands at 426 nm for the Y(B10)F/Q(E11)V mutant and 427 nm for the Y(B10)L/Q(E11)V mutant with shoulders at 438 nm and electronic transitions in the visible region at 527 (sh) and 559 nm. As shown in the inset in Figure 2A (Supporting Information), the second derivative spectra of the Soret region displayed a single band at 437 nm for wild-type trHbN and two bands centered at 438 and 424 nm for the double mutants, which indicated a mixture of a 5C (λ_{max} = 438 nm) and a six-coordinate (6C) species (λ_{max} = 424 nm).

High-Frequency Resonance Raman Spectra of the Deoxy Derivatives. The high-frequency region (1300−1700 cm^{-1}) of the resonance Raman spectra of hemeproteins are comprised of several porphyrin in-plane vibrational modes, which are sensitive to the oxidation, coordination, and spin-state of the heme iron (*26*−*28*). As shown in Figure 1A, the high-frequency resonance Raman spectra of the Y(B10)F, Y(B10)L (*11*), Q(E11)V, and Y(B10)L/Q(E11)V mutants were very similar to that of wild-type trHbN and typical of a deoxy 5C high-spin species with a ν_4 line near 1353 cm^{-1} and a ν_3 line near 1468 cm^{-1} (Table 1). The spectrum of the deoxy Q(E11)A mutant showed an additional band at 1372 cm^{-1} (ν_4) that represented a shoulder in the wild-type protein (Figure 1A). No corresponding spin/coordination band ν_3 was detected at pH 7.5 for that population. The frequency of this supplementary ν_4 line was similar to that reported for the four-coordinated (4C) deoxy *Chlamydomonas* trHb at pH 5.0 (*29*) with ν_4 and ν_3 lines at 1373 and 1499 cm^{-1}, respectively. We thus recorded the deoxy spectra at pH 5.0 of both wild-type trHbN and the Q(E11)A mutant (Figure 1B and Table 1). The acidic form of wild-type trHbN was characterized by a mixture of two species with ν_4 lines at 1353 and 1372 cm^{-1} and ν_3 lines at 1468 and 1503 cm^{-1}, which correspond to a 5C and 4C species, respectively. In contrast, the deoxy spectrum of the Q(E11)A mutant revealed a 4C species (ν_4 = 1372 cm^{-1}; ν_3 = 1503 cm^{-1}) with a minor contribution from a 5C population (ν_4 = 1353 cm^{-1}; ν_3 = 1468 cm^{-1}).

The high-frequency region of the resonance Raman spectrum of the deoxy Y(B10)F/Q(E11)V mutant showed at pH 7.5 a predominant 5C population with ν_4 at 1354 cm^{-1} and ν_3 at 1470 cm^{-1} (Figure 1A). It also revealed an additional ν_3 line at 1494 cm^{-1}, a frequency not found in the deoxy spectra of the wild-type protein and the other (Y(B10)L/Q(E11)V) double mutant (Table 1). The frequency of that ν_3 line was similar to that reported for the 6C deoxy species where the sixth coordination position is occupied by an endogenous ligand (*29*). Changing the wavelength of the excitation light to 413.1 nm enhanced the contribution of the 6C species to the deoxy spectra of both double mutants as revealed by the ν_4 and ν_3 frequencies located at 1362 cm^{-1} (sh) and 1490 cm^{-1}, respectively, for the Y(B10)F/Q(E11)V mutant and at 1365 cm^{-1} (sh) and 1493 cm^{-1} (sh), respectively, for the Y(B10)L/Q(E11)V mutant (Table 1).

Low-Frequency Resonance Raman Spectra of the Deoxy Derivatives. In addition to several in-plane and out-of-plane vibrational modes of the heme porphyrin ring, the low-frequency region of the resonance Raman spectra of heme proteins contains the vibrational modes associated with the coordinated ligands of the heme iron (*26*−*27*). The assignment of a ligand vibrational mode is extremely useful because

Table 1: Frequencies of the Vibrational Modes of the Deoxy, O_2, and CO Derivatives of TrHbN and Its Mutants

Protein	ν_{Fe-His}	Deoxy pH 7.5	Deoxy pH 5	ν_{Fe-OO}	ν_{Fe-CO}	ν_{C-O}	References
trHbN	224	ν_4 : 1353 ν_3 : 1468 ν_4 : 1372 sh[f]	ν_4 : 1353 ν_3 : 1468 ν_4 : 1372 ν_3 : 1503	562	500, 534	1948, 1917	*11*, this work
Y(B10)F	226	ν_4 : 1353 ν_3 : 1468	ν_4 : 1353 ν_3 : 1468	564	501	1949, 1937	*11*, this work
Y(B10)L	226	ν_4 : 1356 ν_3 : 1471	n.d.[d]	572	501	1951	*11*, this work
Q(E11)V	224	ν_4 : 1355 ν_3 : 1470	ν_4 : 1355 ν_3 : 1470	568	487, 523	n.a.[e]	this work
Q(E11)A	225	ν_4 : 1355 ν_3 : 1470 ν_4 : 1372	ν_4 : 1353 sh ν_3 : 1468 ν_4 : 1372 ν_3 : 1503	562	527	1925	this work
Y(B10)F / Q(E11)V	223	ν_4 : 1354 [a] ν_3 : 1470 ν_3 : 1494	ν_4 : 1354 ν_3 : 1470	564 [c]	493	1950	this work
Y(B10)L / Q(E11)V	220	ν_4 : 1354 [b] ν_3 : 1470	n.d.	566	485	1967	this work

[a] The spectrum acquired with the 413.1 nm line of a krypton ion laser showed two ν_4 at 1355 and 1362 cm^{-1} (sh) with corresponding ν_3 at 1470 and 1490 cm^{-1}, respectively. [b] The spectrum acquired with the 413.1 nm line of a krypton ion laser showed two ν_4 at 1355 and 1365 cm^{-1} (sh) with corresponding ν_3 at 1470 and 1490 cm^{-1}, respectively. [c] The Fe−O−O bending mode was detected at 425 cm^{-1}. [d] n.d.: not determined. [e] n.a.: not available due to high fluorescence background. [f] sh: shoulder.

it directly identifies a particular ligand and the nature of its interactions with amino acid residues in the heme pocket. In particular, the proximal Fe−His stretching mode (ν_{Fe-His}) can be identified in the 5C deoxy forms of hemoglobins in the 200−250 cm^{-1} region. The frequency of the ν_{Fe-His} mode of the deoxy form at pH 7.5 of the single mutants (224−226 cm^{-1}) and the double YB10F/QE11V (226 cm^{-1}) mutant was found to be nearly identical to that of wild-type trHbN (224 cm^{-1}) (Figure 2), indicating no proximal strain or a weak one on the Fe−His bond in these proteins (Table 1). In contrast, the ν_{Fe-His} mode at 220 cm^{-1} of the deoxy Y(B10)L/Q(E11)V mutant, which was identical to that of myoglobin, indicated a weaker Fe−His bond that may be attributed to the additional proximal strain or to a weakened electronic coupling between the orbitals of the H(F8) and those of the heme iron (Figure 2 and Table 1). Hence, the significant change in the Fe−His stretching mode for the Y(B10)L/Q(E11)V mutant is compelling evidence that the heme positioning or the mini-F helix positioning is highly responsive to the architecture of the distal heme pocket.

O_2-Bound Derivatives. We have studied the oxy complex of the trHbN mutants by resonance Raman spectroscopy with the aim of assigning the Fe−O_2 stretching mode (ν_{Fe-OO}) and determining its sensitivity to the environment in the heme pocket. The frequency of the ν_{Fe-OO} mode directly reflects the strength of the Fe−O_2 bond. Figure 3 compares the low-frequency region of the resonance Raman spectra of the oxy adducts of wild-type trHbN and its mutants. Each Fe−O_2 stretching mode assignment was confirmed by isotope ($^{18}O_2$) substitution experiments. As previously reported (*11*), a single ν_{Fe-OO} mode, located at 562 cm^{-1}, was observed in trHbN (Figure 3 a, b, c). The low ν_{Fe-OO} frequency in trHbN indicated a constrained and weakened Fe−O_2 bond because of hydrogen bonding between the Y(B10) hydroxyl and the proximal oxygen atom of the bound O_2, a model that has been supported by the crystalline structure of oxy-trHbN (Figure 6A) (*7*). The ν_{Fe-OO} mode shifted to 572 cm^{-1} when Y(B10) was substituted with leucine (Figure 3 m, n, o), a frequency that has been observed in vertebrate myoglobins and hemoglobins. In contrast, replacing Y(B10) with a phenylalanine caused only a small shift in the ν_{Fe-OO} mode to 564 cm^{-1} indicating strong interaction with the proximal oxygen (Figure 3 j, k, l).

Replacing Q(E11) with the small nonpolar residue alanine did not alter the ν_{Fe-OO} mode, which was still located at 562 cm^{-1} (Figure 3 d, e, f). In contrast, the isosteric Q(E11)V substitution shifted the ν_{Fe-OO} mode to 568 cm^{-1} indicating that the Fe−O_2 bond is no longer constrained by Y(B10) residue (Figure 3 g, h, i).

The ν_{Fe-OO} modes of the Y(B10)F/Q(E11)V (Figure 3 p, q, r) and Y(B10)L/Q(E11)V (Figure 3 s, t, u) mutants were located at 564 and 566 cm^{-1}, respectively, which indicated that there was still significant interaction with the proximal oxygen. Interestingly, the Fe−O_2 bending mode was detected

Table 2: Data Collection and Refinement Statistics for the Mutant trHbN Structures Presented

	Q(E11)A	Q(E11)V	Y(B10)F	Y(B10)F/ Q(E11)V
data collection	Desy BW7B	ESRF ID14-1	Desy BW7B	ESRF ID14-3
indexing/ scaling	Denzo/ Scalepack	Mosflm/ Scala	Mosflm/ Scala	Mosflm/ Scala
resolution range (Å)	50.0−1.98	40.5−2.10	30.1−1.72	45−1.91
mosaicity (°)	1.04	1.80	0.45	0.80
completeness (%)	99.9 (98.0)[a]	73.2 (69.9)[b]	97.1 (82.0)[c]	95.2 (76.7)[d]
R-merge (%)	14.9 (43.8)	14.3 (64.7)	3.6 (19.3)	6.4 (35.8)
unique reflections	17563	11229	27177	18928
average $I/\sigma(I)$	13.7 (4.3)	7.8 (1.4)	13.1 (3.8)	16.2 (2.5)
multiplicity	7.0 (6.4)	2.5 (2.4)	3.7 (3.6)	3.8 (2.5)
no. of active protein atoms	1956	1899	1903	1932
no. of solvent and other nonprotein atoms	294	138	423	300
R-factor/R-free (%)[e]	17.8/23.9	20.5/28.6	18.6/22.8	17.3/23.1
rmsd from ideal geometry				
bond lengths (Å)	0.012	0.009	0.015	0.012
bond angles (°)	1.28	1.20	1.39	1.27
Ramachandran plot[f]				
most favored region (%)	96.8	97.7	97.2	98.1
additional allowed regions (%)	3.2	2.3	2.8	1.9

[a] Values for the outermost shell (2.24−2.00). [b] Values for the outermost shell (2.21−2.10). [c] Values for the outermost shell (1.80−1.72). [d] Values for the outermost shell (2.02−1.91). [e] Calculated using 5% of the reflections. [f] Data produced with the program PROCHECK (*60*).

at 425 cm^{-1} for the Y(B10)F/Q(E11)V mutant, a frequency similar to that of human hemoglobin (*30*) (Figure 3 p, q, r and Table 1). For all proteins, the magnitude of the isotopic shift was in the 21−26 cm^{-1} range, very close to the 24 cm^{-1} isotopic shift expected for a diatomic oscillator.

CO-Bound Derivatives. The Fe−CO stretching mode (ν_{Fe-CO}) is sensitive to the nature of distal interactions with CO and is also dependent on the nature of the proximal ligand. Figure 4 shows the low-frequency region of the resonance Raman spectra of the CO adduct of wild-type trHbN and its mutants. Each of these assignments was confirmed by isotope ($^{13}C^{18}O$) substitution experiments.

In accordance with our previous work, two ν_{Fe-CO} modes were observed at 500 and 534 cm^{-1} in wild-type trHbN (ref 11(*11*) and Figure 4 a, b, c). The frequency of the mode at 534 cm^{-1} indicated a positive polar interaction and was interpreted as originating from a conformation in which the distal Y(B10) interacts with the heme-bound CO. The ν_{Fe-CO} mode at 500 cm^{-1} was assigned to a conformation that did not involve this electrostatic interaction. Accordingly, the replacement of Y(B10) by aromatic (phenylalanine) (Figure 4 j, k, l) or aliphatic (leucine) (Figure 4 m, n, o) amino acids produced a single ν_{Fe-CO} mode located at 501 cm^{-1} (ref 11 and Table 1).

Interestingly, the Q(E11)A (Figure 4 d, e, f) and Q(E11)V (Figure 4 g, h, i) mutants displayed a ν_{Fe-CO} mode at 527 and 523 cm^{-1}, respectively. The 4 cm^{-1} difference in the frequency of the ν_{Fe-CO} mode, between the Q(E11)A and the Q(E11)V mutants, suggested that the size of the E11 residue may modulate the interaction of Y(B10) with the bound CO. In addition to the ν_{Fe-CO} mode at 523 cm^{-1}, the Q(E11)V mutant displayed a second ν_{Fe-CO} mode at 487 cm^{-1} that was nearly identical to that observed for the Y(B10)L/Q(E11)V double mutant (Figure 4 s, t, u). When both B10 and E11 residues were replaced with nonpolar residues such as those in the Y(B10)F/Q(E11)V (Figure 4 p, q, r) and Y(B10)L/Q(E11)V mutants (Figure 4 s, t, u), a single ν_{Fe-CO} mode was observed at 493 and 485 cm^{-1}, respectively. The Fe−CO stretching modes in these mutants indicate an open distal heme pocket with no positive interaction with the bound CO.

The magnitude of the ν_{Fe-CO} isotopic shifts for wild-type trHbN, the Q(E11)A, Y(B10)L and double mutants, are in the 13−16 cm^{-1} range, very close to the 16 cm^{-1} isotopic shift expected for a diatomic oscillator. In contrast, the Q(E11)V (523 cm^{-1}) and Y(B10)F (501 cm^{-1}) mutants exhibit larger isotopic shifts, 19 and 21 cm^{-1}, respectively. Previous studies showed that a lowering of the mass of the iron-ligand system, caused by an increase in the angular distortion of the iron−ligand moiety results in larger isotopic shifts (*31*, *32*). Hence, the shifts of the ν_{Fe-CO} modes for the latter mutants may reflect important deformations of the Fe−C−O bond. The small 10 cm^{-1} shift of the lower ν_{Fe-CO} mode (487 cm^{-1}) of the Q(E11)V mutant is attributed to the overlapping of porphyrin modes with the ν_{Fe-CO} band, which hampers the precise determination of the isotopic shift.

In the high-frequency region (Figure 5 and Table 1), two C−O stretching modes (ν_{C-O}) at 1917 and 1948 cm^{-1} were detected for wild-type trHbN (Figure 5 a, b, c), which correspond to the 534 and 500 cm^{-1} Fe−CO stretching modes, respectively. Two ν_{C-O} modes at 1937 (minor) and 1949 cm^{-1} (major) were also observed for the Y(B10)F mutant (Figure 5 g, h, i). A single C−O stretching mode (ν_{C-O}) was detected at 1925, 1950, 1951, and 1967 cm^{-1}

for the Q(E11)A (Figure 5 d, e, f), Y(B10)F/Q(E11)V (Figure 5 m, n, o), Y(B10)L (Figure 5 j, k, l) and Y(B10)L/Q(E11)V (Figure 5 p, q, r) mutants, respectively. The 16 cm^{-1} isotopic shift between the bands located at 1861 cm^{-1} ($^{12}C^{16}O$) and 1845 cm^{-1} ($^{13}C^{18}O$) in the Y(B10)L/Q(E11)V difference spectrum (Figure 5 r) was attributed to an overtone of the ν_{Fe-CO} mode mixed with the ν_4 line at 1372 cm^{-1} (*33*). The C−O stretching mode for the Q(E11)V mutant could not be properly assigned because of a high fluorescence background. For all proteins, the magnitude of the ν_{C-O} isotopic shift was in the 86−91 cm^{-1} range, very close to the 90 cm^{-1} isotopic shift expected for a diatomic oscillator.

Because of the electronic structure of the Fe−C−O moiety, an inverse correlation between the stretching frequencies of the Fe−CO and C−O stretching modes occurs in hemeproteins. As a result, an increase of the Fe−CO stretching mode correlates with a decrease of the C−O stretching mode and vice versa. The correlation between these two stretching modes depends on the presence and nature of the proximal ligand (*34*, *35*). Back-bonding to C−O is modulated by many factors, such as the polarity of the distal environment and steric crowding of the bound ligand. (*34*). The ν_{Fe-CO} and ν_{C-O} frequencies of all studied proteins fall on the imidazole/histidine correlation curve indicating no significant change in the nature and character of the proximal ligand (Figure 3, Supporting Information).

The ν_{Fe-CO} and ν_{C-O} frequencies of the Y(B10)-CO conformation of wild-type trHbN (534 cm^{-1}) and those of the Q(E11)A mutant are located in the upper left part of the correlation curve, which indicate high back-bonding because of strong or multiple positive distal interactions with the bound CO. In contrast, the ν_{Fe-CO} and ν_{C-O} frequencies of the Y(B10)L, Y(B10)F (1949 cm^{-1}), and the Y(B10)F/Q(E11)V mutants are found in the region corresponding to the conformation of wild-type trHbN associated to the lower ν_{Fe-CO} mode (500 cm^{-1}), reflecting a decrease in back-bonding because of weak positive interactions with the ligand. The Y(B10)L/Q(E11)V mutant occupies the lower end of the correlation curve, indicating an apolar environment surrounding the bound CO (*12*, *34*, *36*−*37*).

Crystal Structures of trHbN Mutants. To examine the structural consequences of individual or joint substitutions at the B10 and E11 sites, we determined the 3D structures of the Y(B10)F, Q(E11)A, Q(E11)V, and Y(B10)F/Q(E11)V trHbN mutants, in their cyano-met forms. Details of the refined crystal structures of the mutant proteins are reported in Table 2. All mutations had little effects on the overall trHbN tertiary structure and on the mutual assembly of the two protein chains present in the crystallographic asymmetric unit. The rmsd values in the 0.24−0.66 Å range (253 Cα pairs) were observed when the full asymmetric unit dimer was compared among the four mutants and in the wild-type protein. In addition, the structural overlay of the A chain in the different mutants and in the wild-type protein yielded rmsd values in the 0.23−0.41 Å range (127 Cα pairs). The latter values are slightly lower than those observed in the comparisons between A and B chains within each of the different trHbN crystal structures considered here (rmsd range 0.67−0.79 Å, 127 Cα pairs), where deviations in the short *N*-terminal helix of A vs B chains account for the higher rmsd.

Table 3: Stereochemical Parameters for Heme-Fe- -Cyanide Coordination in the Four Mutant trHbs

	Y(B10)F	Q(E11)V	Q(E11)A	Y(B10)F/ Q(E11)V
Fe- - -CN distance (Å)	(A) 2.12 (B) 2.04	(A) 2.33 (B) 2.53	(A) 2.31 (B) 2.11	(A) 2.10 (B) 2.18
Fe- - -C- - -N angle (°)	(A) 169 (B) 166	(A) 139 (B) 104	(A) 153 (B) 165	(A) 176 (B) 169
Fe- - -HisF8 distance (Å)	(A) 2.06 (B) 2.05	(A) 2.20 (B) 2.03	(A) 2.10 (B) 2.01	(A) 2.12 (B) 2.07
residue(s) H-bonded to CN^-	Q(E11)	Y(B10)	Y(B10)	
H-bond length	(A) 2.89 (B) 3.03	(A) 2.73 (B) 2.77	(A) 2.67 (B) 2.41	

An inspection of the heme distal site region in the Y(B10)F mutant structure indicated that the overall aromatic side chain conformation was maintained at the mutation site, the largest shift in the benzene ring of F(B10) relative to that of Y(B10) being about 0.3 Å. However, the absence of the phenolic O atom resulted in the loss of a hydrogen bond to the Q(E11) residue, whose side chain readjusts with a shift of 1.9 Å at the CG atom, and in the loss of a hydrogen bond between the B10 residue and the cyanide ligand. A hydrogen bond between Q(E11) NE2 atom and the bound cyanide ligand was, however, maintained (2.89 Å) (Figure 6C). The cyanide coordination geometry appeared to be affected by the loss of the B10 phenolic O atom, mainly through a relaxation of the coordination bond to the heme Fe atom, which was longer by about 0.2 Å in both chains of the Y(B10)F mutant, relative to that of the the wild-type protein (Table 3).

No distal site water molecules were present in either the wild-type protein or the Y(B10)F mutant structures, thus preventing possible compensating mechanisms for ligand hydrogen bonding within the heme distal cavity. As additional detail in the context of the observed structural perturbations, we noted that residue F(E15), adopting two distinct conformations in wild-type trHbN, is frozen in one of the two in the Y(B10)F mutant (Figure 6 A, C). The conformation adopted in both asymmetric unit chains corresponds to the so-called open gate structure (the E15 phenyl ring is roughly parallel to the heme plane) in relation to the possible gating role exerted by F(E15) within the apolar tunnel traversing the protein matrix in trHbN. Relative to such an issue, it should be noted that the F(E15) double side chain conformation observed in wild-type trHbN is equally observed in the 3D structure of the F(CD1)L mutant (Milani and Bolognesi, unpublished results). In this case, in fact, the mutation occurs at a site far from the distal E11 region, leaving unaltered all of the intramolecular interactions supporting the observed F(E15) double conformer.

The Q(E11)V mutation also introduced an evident perturbation of the distal site hydrogen-bonding scheme. As a result of the presence of the apolar Val residue at site E11, the cyanide ligand coordination was perturbed, leading to a looser Fe- - -C coordination bond. The observed Fe - - -C bond lengths (2.33 Å in chain A and 2.53 Å in chain B) were barely compatible with an intact coordination bond. Such loosened coordination bonds are indicative, at least for chain B, of the partial reduction of the Fe center during X-ray data collection, a fraction of the cyanide ion being released but nevertheless trapped by local interactions within the distal

site pocket. As previously reported for several distinct hemeproteins (*38*), such an interpretation is in keeping with the observation of a substantially bent orientation of the cyanide ion in Q(E11)V. The cyanide ligand, however, maintains a strong hydrogen bond to residue Y(B10) in both chains (Table 3); the conformation of Y(B10) is virtually unperturbed by the E11 mutation in both chains. As for the Y(B10)F mutant, only one conformation is observed for the protein matrix tunnel residue F(E15) (in both A and B chains). The E15 phenyl ring orientation differs by about 20° relative to the open gate conformation identified in the wild-type protein; in the mutant, a van der Waals contact to the Q(E11)V residue (a Cβ branched side chain) is the likely factor defining the F(E15) side chain conformation.

Similar conclusions can be drawn for the distal site structure in the Q(E11)A mutant (Table 3). Here, the main notable difference was a slightly altered orientation of the phenyl ring in residue F(E15). In fact, in relation to the smaller size of the A(E11) residue, no van der Waals contacts between residues F(E15) and A(E11) are established, and the F(E15) phenyl ring is observed in the open gate conformation seen in the Y(B10)F mutant (Figure 6C). In addition, also related to the decreased size of the E11 residue, the distal residue L(E7), shifted by one turn along the E-helix, displayed two distinct conformations in chains A and B, none of which appeared to affect the neighboring distal site residues. The stereochemistry of cyanide coordination is also markedly affected in the case of the Q(E11)A mutant (Table 3); a partial reduction of the heme Fe atom during X-ray data collection is a likely factor in this respect.

The structural effects introduced by the Y(B10)F/Q(E11)V double mutation can be schematized as the sum of local perturbations brought about independently by the single-site mutations described above. Thus, essentially, residue F(E15) adopts the conformation reported for the Q(E11)V mutant (i.e., not fully open), and the cyanide ligand, fully devoid of hydrogen bonding interactions in this case, is loosely coordinated to the heme Fe atom, in a tilted orientation (Table 3 and Figure 6D).

DISCUSSION

Ferric Derivative. In contrast to the wild-type protein and B10-site trHbN mutants, all of which display optical spectra typical of 6C high-spin ferric forms at neutral pH, those of the Q(E11) mutants revealed a predominant 6C low-spin species. The signatures of the ferric spectra of the Q(E11) mutants with bands near 410, 545, and 580 nm are similar to those of trHbN at pH 10.5 (410, 543, and 578 nm), where an hydroxyl ion is coordinated to the heme iron (*11*). Lochner et al. (*39*) showed that the origin of the low-spin state of ferric cytochrome $P450_{cam}$ is due to the deprotonation of the bound water molecule by oxygen atoms that are close to the iron-bound ligand. Hence, we propose that in the absence of Q(E11), the nonbonded electrons from the Y(B10) hydroxyl oxygen may be free to interact and deprotonate the bound water molecule, thus imparting a low-spin character to the iron-coordinated ligand. In this respect, we note that partial disruption of the distal site hydrogen-bonding network induced by the mutated apolar residues at site E11 may have remarkable effects on Y(B10) side chain reactivity, affecting at the same time the conformation and dynamics of the tunnel gating residue F(E15).

The 5C ferric spectra at pH 7.5 of both B10−E11 double mutants are similar to those of *Aplysia limacina* myoglobin at neutral pH (*40*) and to those of the H(E7)V (392 nm), H(E7)M (395 nm), and H(E7)F (393 nm) sperm whale myoglobin mutants, which do not display any water molecule bound to the heme distal site (*41*). The above observations suggest that the Y(B10)−Q(E11) pair controls the binding and the ionization state of the bound water in ferric trHbN. Such considerations are further supported by the crystal structures of the cyano-met derivatives of wild-type and mutant trHbN, which show the direct involvement of either Y(B10) or Q(E11), or both in hydrogen bonds to the heme-bound ligand (ref 16 and Figure 6B). Remarkably, such hydrogen-bonding capabilities are displayed in the crystal structures even when cyanide is loosely coordinated to the heme Fe-atom.

Ferrous Derivative. The optical and the resonance Raman spectra showed that in the deoxy wild-type trHbN and in the single-site B10 and E11 mutants, the sixth coordination position is vacant. In contrast, both double-site mutants present a mixture of 5C and 6C species. An inspection of the crystal structure of oxy-trHbN and those reported here does not point to a distal residue that could coordinate to the heme Fe-atom without imposing a significant conformational rearrangement of the distal heme pocket. Major conformational changes involving the motion of both E and B helices have been reported upon cyanide and azide binding to ferric 6C *Synechocystis* trHb (*8*). For the latter protein, such movements are regulated by the substantial reorganization of hydrogen bonds between the heme-D-propionate and the EF hinge region, a process so far not reported for trHbN, whose backbone dynamics is mainly accounted by the movements of the B and E helices (*18*). Taken together, our results indicate that Y(B10) and Q(E11) jointly contribute in keeping the heme sixth coordination position vacant in deoxy trHbN.

A minor 4C population with a stretching frequency at 1372 cm^{-1} was detected in deoxy trHbN at pH 7.5 and becomes dominant at pH 5.0 in the Q(E11)A mutant. No 4C species was detected at pH 7.5 for the single Y(B10) and the double B10/E11 mutants indicating that the Y(B10) hydroxyl is involved in the weakening of the Fe−His bond. In addition, the presence of a bulky apolar side chain at the E11 position (Q(E11)V) impairs the Y(B10) hydroxyl-mediated Fe−His bond destabilization. In deoxy myoglobin, the formation of a stable 4C species occurs at acidic pH (<3.5), driven primarily by low pH-induced conformational fluctuations, which weaken the Fe−His bond, and from the protonation of the proximal F8 histidine (*42*). These observations suggest that in deoxy trHbN, the Q(E11) residue plays an important role in maintaining the integrity of the proximal Fe−His bond through sterically and electronically restraining the Y(B10) hydroxyl.

Structural Interpretation of the Vibrational Conformers of the O_2 Derivatives. The Fe−O_2 complex of hemoglobins is polar with a conformation that appears to be predominantly $Fe^{3+}-O-O^-$, where the electron density of the Fe atom is delocalized toward the distal oxygen of the complex (*33*, *43*). As a result, the Fe−O_2 stretching frequency is relatively insensitive to electrostatic interactions with the distal residues. In contrast, the Fe−O_2 stretching frequency of trHbN is very sensitive to the Y(B10) mutation. In oxygenated

trHbN, Y(B10) interacts directly with the proximal oxygen atom of the bound O_2 (hydrogen bonds of 3.1 Å, in both A and B chains), likely constraining and weakening the Fe−O_2 bond as indicated by a low ν_{Fe-OO} frequency (*11*). Substituting Y(B10) for Leu releases the proximal oxygen atom of the bound oxygen, and as a result, the ν_{Fe-OO} mode shifts to a frequency similar to that in the vertebrate myoglobins and hemoglobins (570 cm^{-1}) (*30*).

Effect of the Single Substitutions at Position E11 on the ν_{Fe-OO}. The ν_{Fe-OO} frequencies of wild-type trHbN and the Q(E11)A mutant are identical, suggesting that in both proteins, the main ligand interaction does not rely on Q(E11). Indeed the (static) crystal structure of oxygenated trHbN shows that the main hydrogen bonding interaction to the O_2 ligand is provided by Y(B10), whose phenolic −OH group is at equal distances from both distal and proximal O atoms of the ligand. Instead, Q(E11), is involved in a hydrogen bond to Y(B10) phenolic −OH but not to the O_2 heme ligand. The crystal structures of both cyano-met Q(E11)A and Q(E11)V mutants clearly indicate that the location of the Y(B10) phenolic O atom is only marginally affected by the mutations. (The observed displacements are in the order of 0.3−0.4 Å, i.e., very close to the rmsd found for protein backbone comparisons.) The resonance Raman spectra, however, show that the Q(E11)V substitution causes an increase of the ν_{Fe-OO} mode to 568 cm^{-1}, a frequency indicating that the Y(B10) residue hardly interacts with the proximal oxygen atom. The 6 cm^{-1} difference in the ν_{Fe-OO} modes of the Q(E11)V and Q(E11)A mutants is likely related to the action of the bulkier V(E11) side chain, which is in van der Waals contact with Y(B10) (in the crystal structure), and may subtly affect its interaction with the proximal oxygen atom. In this respect, it should be noted that the Q(E11)V substitution not only adds a bulky residue (branched at Cβ) in the distal cavity, but it also alters the H-bonding network to the ligand. The data thus suggest that the fine-tuning of the Y(B10) position or orientation, hardly observable in the crystal structures, may prevent the interaction of the Y(B10) hydroxyl with the proximal O atom. Altogether, the above observations indicate that the combination of size and polarity for the E11 residue is critical for the correct positioning of Y(B10), the primary interacting residue required to stabilize the bound oxygen molecule.

Effect of the Single Substitutions at Position B10 on the ν_{Fe-OO}. Interestingly, replacing Y(B10) with phenylalanine caused a small shift in the Fe−O_2 stretching frequency from 562 to 564 cm^{-1}, a frequency much lower than that observed for the Y(B10)L mutant (572 cm^{-1}), indicating a strong interaction with the bound O_2 that is attributed to the positive edge of the phenyl multipole. Indeed, an analysis of the cyano-met Y(B10)F mutant crystal structure is in agreement with the above interpretation; the closest distance (in the two chains) of the F(B10) phenyl ring and the distal atom of the biatomic ligand is 3.2 Å, in line with the establishment of an aromatic−electrostatic interaction. Such productive electrostatic interaction has also been described in the L(B10)F myoglobin mutant (*43*−*45*).

Effect of the Double Substitutions at Position B10 and E11 on the ν_{Fe-OO}. The Fe−O_2 stretching mode at 564 cm^{-1} for the Y(B10)F/Q(E11)V mutant is identical to that of the Y(B10)F mutant, supporting the involvement of F(B10) in oxygen stabilization through aromatic−electrostatic interactions and revealing that the hydrogen bond between Q(E11) and the distal oxygen atom of the iron-bound ligand, as shown in the cyanomet crystal structure of the Y(B10)F mutant, does not alter the Fe−O_2 stretching mode. However, when the B10 phenylalanine is replaced by leucine achieving the Y(B10)L/Q(E11)V mutant, the Fe−O_2 stretching frequency increases to 566 cm^{-1}, a value that is still relatively low. It is possible that the conformational changes underlying the presence of a 6C population in the deoxy form of both double mutants may force an unidentified distal pocket residue to come in close proximity to the bound oxygen and strongly interact with it.

Structural Interpretation of the Vibrational Conformers of the CO Derivatives. In hemeproteins, the iron-coordinated CO molecule is a suitable probe to study changes in the structural and electrostatic environments occurring in the distal binding pocket. Ligand sensitivity evolves from its lone pair of electrons that is delocalized when CO is near charged groups (*33*). As a result, when CO is near a positively charged group, the $Fe^{+}{=}C{=}O^{-}$ tautomer is stabilized, in which the Fe−CO and C−O bonds have a double bond character, and the ligand oxygen has a partial negative charge. In contrast, when CO is near a negatively charged group, the $Fe^{-}{-}C{\equiv}O^{+}$ tautomer is stabilized, in which the Fe−CO bond leans toward a single bond character, and the C−O tends toward a triple bond character, whereas the ligand oxygen has a partial positive charge (*33*, *46*). Moreover, there is an inverse correlation between the stretching frequencies of Fe−CO and C−O arising from the π-electron back-donation from the $d\pi_{(dxz,dyz)}$ orbitals of the iron to the empty π^* orbitals of CO (*47*−*49*). As a result, an increase of the Fe−CO bond order correlates with a decrease of the C−O bond order and vice versa. The correlation between these two stretching modes depends on the nature or the absence of the proximal ligand (*34*, *35*). Back-bonding to CO is modulated by many factors, such as the polarity of the distal environnement, the steric crowding of the bound ligand, and the electrostatic interactions with the CO oxygen (*34*).

Effect of the Single Substitution at Position E11 on the ν_{Fe-CO}. We previously showed that like cytochrome *c* peroxidase (*50*), *Escherichia coli* flavohemoglobin HMP (*37*), *Ascaris suum* hemoglobin (*47*, *51*), barley nonsymbiotic hemoglobin (*34*), and human neuroglobin (*33*) the distal heme pocket of wild-type CO-trHbN is in an equilibrium between two conformational states, reflected by two ν_{Fe-CO} modes at 500 and 534 cm^{-1}, respectively, and their corresponding ν_{C-O} stretching frequencies at 1948 and 1917 cm^{-1}, respectively (*11*). The higher frequency of the Fe−CO stretching mode at 534 cm^{-1}, which is characteristic of a highly polar distal environment, was proposed to arise from a strong electrostatic interaction between the B10 tyrosine hydroxyl and the ligand oxygen stabilizing a structure tending toward the $Fe^{+}{=}C{=}O^{-}$ form (*11*). The lower Fe−CO stretching frequency at 500 cm^{-1} was attributed to a conformation lacking this strong hydrogen-bonding interaction, characteristic of a less polar-binding pocket.

Substitution of the Q(E11) residue by alanine and valine revealed a single Fe−CO stretching mode at 527 and 523 cm^{-1}, respectively, indicating that the Y(B10) hydroxyl strongly interacts with the heme-bound CO in all trHbN molecules, stabilizing a structure tending toward the $Fe^{+}{=}C{=}O^{-}$ form. The latter observation is consistent with

the crystal structures of these mutants, which reveal a strong interaction between the bound CN and Y(B10). As mentioned previously, the lower Fe−CO stretching frequency at 487 cm^{-1} displayed by the Q(E11)V mutant is characteristic of a hemoglobin or myoglobin with an open heme pocket with no positive groups interacting directly with the bound CO, suggesting that the bulkier E11 valine side chain steers the Y(B10) hydroxyl away from ligand. We suggest that the hydrogen bond connecting the Q(E11) and the Y(B10) residues in wild-type trHbN controls the strength of the electrostatic interaction between Y(B10) and the bound CO. In contrast, in *Cerebratulus* mini-hemoglobin, T(E11) orients the Y(B10) hydroxyl oxygen nonbonded electrons toward the bound CO, which hinders a strong positive electrostatic interaction between the tyrosine B10 hydroxyl hydrogen and the ligand (ν_{C-O} = 1979 cm^{-1}) (*52*). Substituting T(E11) in *Cerebratulus* mini-hemoglobin for a nonhydrogen-bond donor residue like valine (ν_{C-O} = 1937 cm^{-1}) or alanine (ν_{C-O} = 1931 cm^{-1}) frees the Y(B10) hydroxyl and enables, as in trHbN (ν_{C-O} = 1917 cm^{-1}), a strong positive electrostatic interaction between Y(B10) hydroxyl and the bound CO.

The 4 cm^{-1} ν_{Fe-CO} frequency difference between the Q(E11)A and the Q(E11)V mutants suggests that the size of the E11 side chain residue fine-tunes the position and orientation of the Y(B10) side chain, therefore controlling the strength of Y(B10) interaction with the iron-bound CO. Thus, as observed for the oxygenated complex, the bulkier Q(E11)V side chain partially releases the CO from its interaction with Y(B10). The lower frequency of the ν_{Fe-CO} in the Q(E11)A mutant (527 cm^{-1}) with respect to that of wild-type trHbN (534 cm^{-1}) indicates a suboptimal interaction between Y(B10) and the heme-bound CO. Thus, not only the size of the Q(E11) residue appears to be important to optimize the Y(B10)−CO interaction but also the hydrogen bond formed between Q(E11) and Y(B10).

Effect on the ν_{Fe-CO} of the Single Substitutions at Position B10 and Double Substitutions at Positions B10 and E11. A single conformation with a ν_{Fe-CO} at 501 cm^{-1} and a ν_{C-O} at 1951 cm^{-1} is observed when the Y(B10) is mutated to leucine (Table 1). The Fe−CO stretching mode frequency indicates that a weak positive polar interaction with the bound CO still exists, possibly with Q(E11). Evidence that the ν_{Fe-CO} mode at 501 cm^{-1} results from an interaction with the Q(E11) residue is provided by the lower Fe−CO stretching frequencies, 493 and 485 cm^{-1}, and their corresponding C−O stretching modes at 1950 and 1967 cm^{-1}, observed for the Y(B10)F/Q(E11)V and Y(B10)L/Q(E11)V double mutants, respectively. Such low frequencies have been reported for *E. coli* HMP (ν_{Fe-CO} = 494 cm^{-1}; ν_{C-O} = 1960 cm^{-1}) (*37*), *Chlamydomonas eugametos* (ν_{Fe-CO} = 490 cm^{-1}; ν_{C-O} = 1957 cm^{-1}) (*29*), *Paramecium caudatum* (ν_{Fe-CO} = 493 cm^{-1}; ν_{C-O} = 1974 cm^{-1}) (*12*), and barley hemoglobin (ν_{Fe-CO} = 493 cm^{-1}; ν_{C-O} = 1960 cm^{-1}) (*34*), where no positive groups contact the heme-bound CO. The 8 cm^{-1} ν_{Fe-CO} frequency difference between the two double mutants indicates that the positive edge of the B10 aromatic multipole can interact with the Fe-bound CO. Such positive multipole interaction is also observed for the CO complexes of the L(B10)F myoglobin mutant (ν_{Fe-CO} = 525 cm^{-1}; wild-type myoglobin = 509 cm^{-1}) and elephant myoglobin (ν_{Fe-CO} = 513 cm^{-1}) (*45*, *53*, *54*). A single conformation with a ν_{Fe-CO} at 501 cm^{-1} is also detected for the Y(B10)F mutant (Table 1). However, two ν_{C-O} bands at 1937 (minor) and 1949 cm^{-1} (major) are observed, suggesting multiple positive interactions with bound CO. Failure to detect two ν_{Fe-CO} bands in the Y(B10)F mutant is attributed to the blending into a single ν_{Fe-CO} band of the Fe−CO stretching frequencies corresponding to the two C−O stretching populations at 1937 and 1949 cm^{-1} and is reflected by the width increase of the ν_{Fe-CO} band (Figure 4 l) compared to that of the Y(B10)L mutant (Figure 4 o). The ν_{Fe-CO} band located at 507 cm^{-1} in the differential spectrum of the Y(B10)F mutant, which decreased to 503 cm^{-1} in the Y(B10)L mutant, is indicative of stronger positive interactions with the bound CO in the former. The crystal structure of the cyano-met Y(B10)F mutant reveals that both the F(B10) phenyl ring and the Q(E11) side chain fall next to the biatomic heme ligand in the context of a rather crowded distal site cavity. Such observation supports, albeit indirectly, the involvement of multiple positive interactions with the bound CO in carbonylated trHbN.

From these results, we propose a model in which trHbN is in a conformational equilibrium where either the Y(B10) or the Q(E11) residue interacts with the heme-bound CO. It is only when the Q(E11) is substituted by a small, nonH-bonding residue that the Y(B10) residue can interact with heme-bound CO in all trHbN molecules giving rise to a single ν_{Fe-CO} mode at a high frequency (527 cm^{-1}). Conversely, when Y(B10) is substituted by a nonH-bonding residue, the heme-bound CO of all trHbN molecules can interact with Q(E11) giving rise to the low-frequency ν_{Fe-CO} mode at 500 cm^{-1}. Presumably, the hydrogen-bond interaction between Y(B10) and Q(E11) fine-tunes the ratio of the two forms in wild-type trHbN. Thus, for both oxygen and CO, the residue at E11 is critical for the control of the interaction between Y(B10) and the heme-bound ligand.

Previous studies revealed that Y(B10) controls the oxygen affinity of *M. tuberculosis* trHbN by stabilizing the iron-bound diatomic ligand (*4*, *11*). However, the X-ray structure showed that the oxygen affinity of trHbN may be controlled by a more complex hydrogen-bonding network involving the Y(B10)/Q(E11) pair (*7*). Here, we extended these observations and showed that Q(E11) plays a key role in modulating the proper interaction of Y(B10) with the proximal oxygen atom of the bound oxygen. Our results also revealed that in ferric trHbN, these two residues control the binding and the ionization state of the heme-bound water molecule. Resonance Raman data indicated that the CO complex of trHbN exists in multiple conformational states, where either Y(B10) or Q(E11) can interact with the bound CO. Taken together, these findings suggest a model describing the behavior of the distal heme pocket of trHbN by which residues Y(B10) and Q(E)11 interact with bound ligands, these interactions being fine-tuned by the same Y(B10)−Q(E)11 pair. Finally, our study suggests that the Y(B10)−Q(E11) pair may play an essential role in the NO detoxification process by allowing the optimal positioning of the substrates and intermediates and by regulating their diffusion out of the active site. In particular, the control exerted by these two residues on the conformation (and presumably on the dynamics) of the protein matrix tunnel gating residue F(E15) may represent an additional key contribution to the molecular processes that sustain the diffusion of diatomic ligands (i.e., O_2 and

NO) to the heme and of their conversion products out of the heme distal pocket within the NO detoxification cycle.

ACKNOWLEDGMENT

We are grateful to Dr. Joel M. Friedman, Dr. Beatrice A. Wittenberg, and Dr. Jonathan B. Wittenberg for insightful discussions.

SUPPORTING INFORMATION AVAILABLE

Optical absorption spectra of the ferric and deoxy complexes of wild-type trHbN and its distal mutants and correlation diagram of the ν_{Fe-CO} and the ν_{C-O} frequencies of various heme proteins having a histidine as the proximal ligand. This material is available free of charge via the Internet at http//pubs.acs.org.

REFERENCES

1. Wittenberg, J. B., Bolognesi, M., Wittenberg, B. A., and Guertin, M. (2002) Truncated hemoglobins: a new family of hemoglobins widely distributed in bacteria, unicellular eukaryotes, and plants, *J. Biol. Chem. 277*, 871−874.
2. Vinogradov, S. N., Hoogewijs, D., Bailly, X., Arredondo-Peter, R., Guertin, M., Gough, J., Dewilde, S., Moens, L., and Vanfleteren, J. R. (2005) Three globin lineages belonging to two structural classes in genomes from the three kingdoms of life, *Proc. Natl. Acad. Sci. U.S.A. 102*, 11385−11389.
3. Lecomte, J. T., Vuletich, D. A., and Lesk, A. M. (2005) Structural divergence and distant relationships in proteins: evolution of the globins, *Curr. Opin. Struct. Biol. 15*, 290−301.
4. Couture, M., Yeh, S. R., Wittenberg, B. A., Wittenberg, J. B., Ouellet, Y., Rousseau, D. L., and Guertin, M. (1999) A cooperative oxygen-binding hemoglobin from *Mycobacterium tuberculosis*, *Proc. Natl. Acad. Sci. U.S.A. 96*, 11223−11228.
5. Ouellet, H., Ouellet, Y., Richard, C., Labarre, M., Wittenberg, B. A., Wittenberg, J. B., and Guertin, M. (2002) Truncated hemoglobin HbN protects *Mycobacterium bovis* from nitric oxide, *Proc. Natl. Acad. Sci. U.S.A. 99*, 5902−5907.
6. Pesce, A., Couture, M., Dewilde, S., Guertin, M., Yamauchi, K., Ascenzi, P., Moens, L., and Bolognesi, M. (2000) A novel two-over-two alpha-helical sandwich fold is characteristic of the truncated hemoglobin family, *EMBO J. 19*, 2424−2434.
7. Milani, M., Pesce, A., Ouellet, Y., Ascenzi, P., Guertin, M., and Bolognesi, M. (2001) *Mycobacterium tuberculosis* hemoglobin N displays a protein tunnel suited for O2 diffusion to the heme, *EMBO J. 20*, 3902−3909.
8. Milani, M., Savard, P. Y., Ouellet, H., Ascenzi, P., Guertin, M., and Bolognesi, M. (2003) A TyrCD1/TrpG8 hydrogen bond network and a TyrB10TyrCD1 covalent link shape the heme distal site of *Mycobacterium tuberculosis* hemoglobin O, *Proc. Natl. Acad. Sci. U.S.A. 100*, 5766−5771.
9. Giangiacomo, L., Ilari, A., Boffi, A., Morea, V., and Chiancone, E. (2005) The truncated oxygen-avid hemoglobin from *Bacillus subtilis*: X-ray structure and ligand binding properties, *J. Biol. Chem. 280*, 9192−9202.
10. Trent, J. T., III, Kundu, S., Hoy, J. A., and Hargrove, M. S. (2004) Crystallographic analysis of synechocystis cyanoglobin reveals the structural changes accompanying ligand binding in a hexacoordinate hemoglobin, *J. Mol. Biol. 341*, 1097−1108.
11. Yeh, S. R., Couture, M., Ouellet, Y., Guertin, M., and Rousseau, D. L. (2000) A cooperative oxygen binding hemoglobin from *Mycobacterium tuberculosis*. Stabilization of heme ligands by a distal tyrosine residue, *J. Biol. Chem. 275*, 1679−1684.
12. Das, T. K., Weber, R. E., Dewilde, S., Wittenberg, J. B., Wittenberg, B. A., Yamauchi, K., Van Hauwaert, M. L., Moens, L., and Rousseau, D. L. (2000) Ligand binding in the ferric and ferrous states of Paramecium hemoglobin, *Biochemistry 39*, 14330−14340.
13. Das, T. K., Couture, M., Ouellet, Y., Guertin, M., and Rousseau, D. L. (2001) Simultaneous observation of the O--- O and Fe- - - O2 stretching modes in oxyhemoglobins, *Proc. Natl. Acad. Sci. U.S.A. 98*, 479−484.
14. Mukai, M., Savard, P. Y., Ouellet, H., Guertin, M., and Yeh, S. R. (2002) Unique ligand-protein interactions in a new truncated hemoglobin from *Mycobacterium tuberculosis*, *Biochemistry 41*, 3897−3905.
15. Ouellet, H., Juszczak, L., Dantsker, D., Samuni, U., Ouellet, Y. H., Savard, P. Y., Wittenberg, J. B., Wittenberg, B. A., Friedman, J. M., and Guertin, M. (2003) Reactions of *Mycobacterium tuberculosis* truncated hemoglobin O with ligands reveal a novel ligand-inclusive hydrogen bond network, *Biochemistry 42*, 5764−5774.
16. Milani, M., Ouellet, Y., Ouellet, H., Guertin, M., Boffi, A., Antonini, G., Bocedi, A., Mattu, M., Bolognesi, M., and Ascenzi, P. (2004) Cyanide binding to truncated hemoglobins: a crystallographic and kinetic study, *Biochemistry 43*, 5213−5221.
17. Dantsker, D., Samuni, U., Ouellet, Y., Wittenberg, B. A., Wittenberg, J. B., Milani, M., Bolognesi, M., Guertin, M., and Friedman, J. M. (2004) Viscosity-dependent relaxation significantly modulates the kinetics of CO recombination in the truncated hemoglobin TrHbN from *Mycobacterium tuberculosis J. Biol. Chem. 279*, 38844−38853.
18. Crespo, A., Marti, M. A., Kalko, S. G., Morreale, A., Orozco, M., Gelpi, J. L., Luque, F. J., and Estrin, D. A. (2005) Theoretical study of the truncated hemoglobin HbN: exploring the molecular basis of the NO detoxification mechanism, *J. Am. Chem. Soc. 127*, 4433−4444.
19. Chartier, F. J., and Couture, M. (2004) Stability of the heme environment of the nitric oxide synthase from Staphylococcus aureus in the absence of pterin cofactor, *Biophys. J. 87*, 1939−1950.
20. Otwinowski, Z., and Minor, W. (1997) Processing of X-ray diffraction data collected in oscillation mode, *Methods Enzymol. 276*, 307−326.
21. CCP4 (Collaborative Computational Project 4) (1994) The CCP4 suite: programs for protein crystallography, *Acta Crystallogr., Sect. D 50*, 760−763.
22. Vagin, A. A., and Teplyakov, A. (1997) An approach to multi-copy search in molecular replacement, *Acta Crystallogr., Sect. D 56*, 1622−1624.
23. Murshudov, G. N., Vagin, A. A., and Dodson, E. J. (1997) Refinement of macromolecular structures by the maximum-likelihood method, *Acta Crystallogr., Sect. D 53*, 240−257.
24. Jones, T. A., Zou, J. Y., Cowan, S. W., and Kjeldgaard, M. (1991) Improved methods for building protein models in electron density maps and the location of errors in these models, *Acta Crystallogr., Sect. A 47*, 110−119.
25. Berman, H. M., Westbrook, J., Feng, Z., Gilliland, G., Bhat, T. N., Weissig, H., Shindyalov, I. N., and Bourne, P. E. (2000) The Protein Data Bank, *Nucleic Acids Res. 28*, 235−242.
26. Spiro, T. G., and Li, X. Y. (1988) Resonance Raman spectroscopy of metalloporphyrins, in *Biological Applications of Raman Spectroscopy* (Spiro, T. G., Ed.) pp 1−37, John Wiley & Sons, Inc., New York.
27. Wang, J., Caughey, W. S., and Rousseau, D. L. (1996) Resonance Raman scattering: A probe of heme protein-bound nitric oxide, in *Methods in Nitric Oxide Research* (Feelisch, M., and Stamler, J., Eds.) pp 427−454, John Wiley & Sons, Inc., New York.
28. Hu, S., Smith, K. S., and Spiro, T. G. (1996**)** Assignment of protoheme resonance Raman spectrum by heme labeling in myoglobin, *J. Am. Chem. Soc. 118*, 12638−12646.
29. Couture, M., Das, T. K., Lee, H. C., Peisach, J., Rousseau, D. L., Wittenberg, B. A., Wittenberg, J. B., and Guertin, M. (1999) Chlamydomonas chloroplast ferrous hemoglobin. Heme pocket structure and reactions with Ligands, *J. Biol. Chem. 274*, 6898−6910.
30. Jeyarajah, S., Proniewicz, L. M., Bronder, H., and Kincaid, J. R. (1994) Low-frequency vibrational modes of oxygenated myoglobin, hemoglobins, and modified derivatives, *J. Biol. Chem. 269*, 31047−31050.
31. Takahashi, S., Ishikawa, K., Takeuchi, N., Ikeda-Saito, M., Yoshida, T., and Rousseau, D. L (1995) Oxygen-bound heme−heme oxygenase complex: Evidence for a highly bent structure of the coordinated oxygen, *J. Am. Chem. Soc. 117*, 6002−6006.
32. Macdonald, I. D. G., Sligar, S. G., Christian, J. F., Unno, M., and Champion, P. M. (1999) Identification of the Fe−O−O bending mode in oxycytochrome P450cam by resonance Raman spectroscopy, *J. Am. Chem. Soc. 121*, 376−380.
33. Couture, M, Burmester, T., Hankeln, T., and Rousseau, D. L. (2001) The heme environment of mouse neuroglobin. Evidence

for the presence of two conformations of the heme pocket, *J. Biol. Chem. 276*, 36377−36382.
34. Das, T. K., Lee, H. C., Duff, S. M., Hill, R. D., Peisach, J., Rousseau, D. L., Wittenberg, B. A., and Wittenberg, J. B. (1999) The heme environment in barley hemoglobin, *J. Biol. Chem. 274*, 4207−4212.
35. Wang, J., Stuehr, D. J., and Rousseau, D. L. (1997) Interactions between substrate analogues and heme ligands in nitric oxide synthase, *Biochemistry 36*, 4595−4606.
36. Spiro, T. G., and Wasbotten, I. H. (2005) CO as a vibrational probe of heme protein active sites, *J. Inorg. Biochem. 99*, 34−44.
37. Mukai, M., Mills, C. E., Poole, R. K., and Yeh, S. R. (2001) Flavohemoglobin, a globin with a peroxidase-like catalytic site, *J. Biol. Chem. 276*, 7272−7277.
38. Bolognesi, M., Rosano, C., Losso, R., Borassi, A., Rizzi, M., Wittenberg, J. B., Boffi, A., and Ascenzi, P. (1999) Cyanide binding to Lucina pectinata hemoglobin I and to sperm whale myoglobin: An X-ray crystallographic study, *Biophys. J. 77*, 1093−1099.
39. Lochner, M., Meuwly M., and Woggon, W. D. (2003) The origin of the low-spin character of the resting state of cytochrome P450cam investigated by means of active site analogues, *Chem. Commun. (Cambridge)* 12, 1330−1332.
40. Giacometti, G. M., Ascenzi, P., Brunori, M., Rigatti, G., Giacometti, G., and Bolognesi, M. (1981*)* Absence of water at the sixth co-ordination site in ferric Aplysia myoglobin, *J. Mol. Biol. 15*, 315−319.
41. Morikis, D., Champion, P. M., Springer, B. A., Egeberg, K. D., and Sligar, S. G. (1990) Resonance Raman studies of iron spin and axial coordination in distal pocket mutants of ferric myoglobin, *J. Biol. Chem. 265*, 12143−12145.
42. Das, K. T., Khan, I., Rousseau, D. L., and Friedman, J. L. (1998) Preservation of the native structure in myoglobin at low pH by sol−gel encapsulation, *J. Am. Chem. Soc. 120*, 10268−10269.
43. Hirota, S., Li, T., Phillips, G. N., Jr., Olson, J. S., Mukai, M., Kitagawa, T. (1996) Perturbation of the Fe−O_2 bond by nearby residues in heme pocket: Observation of ν_{Fe-O2} Raman bands for oxymyoglobin mutants, *J. Am. Chem. Soc. 118*, 7845−7846.
44. Springer, B. A., Sligar, S. G., Olson, J. S., and Phillips, N. Jr. (1994) Mechanisms of ligand recognition in myoglobin, *Chem. Rev. 94*, 699−714.
45. Zhao, X., Vyas, K., Nguyen, B. D., Rajarathnam, K., La Mar, G. N., Li, T., Phillips, G. N., Jr., Eich, R. F., Olson, J. S., Ling, J., and Bocian D. F. (1995) A double mutant of sperm whale myoglobin mimics the structure and function of elephant myoglobin, *J. Biol. Chem. 270*, 20763−20774.
46. Phillips, G. N., Jr., Teodoro, M. L., Li., T., Smith, B., and Olson, J. S. (1999) Bound CO is a molecular probe of electrostatic potential in the distal pocket of myoglobin, *J. Phys. Chem. B 103*, 8817−8829.
47. Das, T. K., Friedman, J. M., Kloek, A. P., Goldberg, D. E., and Rousseau, D. L. (2000) Origin of the anomalous Fe−CO stretching mode in the CO complex of *Ascaris* hemoglobin, *Biochemistry 39*, 837−842.
48. Park, K. D., Guo, K. M., Adebodun, F., Chiu, M. L., Sligar, S. G., and Oldfield, E. (1991) Distal and proximal ligand interactions in heme proteins: correlations between C−O and Fe−C vibrational frequencies, oxygen-17 and carbon-13 nuclear magnetic resonance chemical shifts, and oxygen-17 nuclear quadrupole coupling constants in C17O- and 13CO-labeled species, *Biochemistry 30*, 2333−2347.
49. Ray, G. B., Li, X. Y., Ibers, J. A., Sessler, J. L., and Spiro, T. G. (1994) How far can proteins bend the FeCO unit? Distal polar and steric effects in heme proteins and models, *J. Am. Chem. Soc. 116*, 162−176.
50. Dasgupta, S., Rousseau, D. L., Anni, H., and Yonetani, T. (1989) Structural characterization of cytochrome *c* peroxidase by resonance Raman scattering, *J. Biol. Chem. 264*, 654−662.
51. Peterson, E. S., Huang, S., Wang, J., Miller, L. M., Vidugiris, G., Kloek, A. P., Goldberg, D. E., Chance, M. R., Wittenberg, J. B., and Friedman, J. M. (1997) A comparison of functional and structural consequences of the tyrosine B10 and glutamine E7 motifs in two invertebrate hemoglobins (*Ascaris suum* and *Lucina pectinata*), *Biochemistry 36*, 13110−13121.
52. Pesce, A., Nardin, I M., Ascenzi, P., Geuens, E., Dewilde, S., Moens, L., Bolognesi, M., Riggs, A. F., Hale, A., Deng P., Nienhaus, G. U., Olson, J. S., and Nienhaus, K. (2004) Thr-E11 regulates O2 affinity in *Cerebratulus lacteus* mini-hemoglobin, *J. Biol. Chem. 279*, 33662−33672.
53. Li, T., Quillin, M. L., Phillips, G. N., Jr., and Olson, J. S. (1994) Structural determinants of the stretching frequency of CO bound to myoglobin, *Biochemistry 33*, 1433−1446.
54. Carver, T. E., Brantley, R. E., Singleton, E. W., Arduini, R. M., Quillin, M. L., Phillips, G. N., Jr., and Olson, J. S. (1992) A novel site-directed mutant of myoglobin with an unusually high O2 affinity and low autoxidation rate, *J. Biol. Chem. 265*, 14443−14450.
55. Kraulis, P. J. (1991) Molscript: a program to produce both detailed and schematic plots of protein structures, *J. Appl. Crystallogr. 24*, 946−950.
56. Merritt, E. A., and Bacon, D. J. (1997) Raster3D Version2: photorealistic molecular graphics, *Methods Enzymol. 277*, 505−524.
57. Couture, M., Das, T. K., Savard, P. Y., Ouellet, Y., Wittenberg, J. B., Wittenberg, B. A., Rousseau, D. L., and Guertin, M. (2000) Structural investigations of the hemoglobin of the cyanobacterium Synechocystis PCC6803 reveal a unique distal heme pocket, *Eur. J. Biochem. 267*, 4770−4780.
58. Anderton, C. L., Hester, R. E., and Moore, J. N. (1997) A chemometric analysis of the resonance Raman spectra of mutant carbonmonoxy-myoglobins reveals the effects of polarity, *Biochim. Biophys. Acta 1338*, 107−120.
59. Cameron, A. D., Smerdon, S. J., Wilkinson, A. J., Habash, J., Helliwell, J. R., Li, T., and Olson, J. S. (1993) Distal pocket polarity in ligand binding to myoglobin: deoxy and carbonmonoxy forms of a threonine68(E11) mutant investigated by X-ray crystallography and infrared spectroscopy, *Biochemistry 32*, 13061−13070.
60. Laskowski, R. A., MacArthur, M. W., Moss, D. S., and Thornton, J. M. (1993) PROCHECK: a program to check the stereochemical quality of protein structures, *J. Appl. Crystallogr. 26*, 283−291.

BI060112O